

available at [www.sciencedirect.com](http://www.sciencedirect.com)[www.elsevier.com/locate/matchar](http://www.elsevier.com/locate/matchar)

# Corrosion of 15th and early 16th century stained glass from the monastery of Batalha studied with external ion beam

M. Vilarigues<sup>a,\*</sup>, P. Redol<sup>a,b</sup>, A. Machado<sup>a</sup>, P.A. Rodrigues<sup>c</sup>, L.C. Alves<sup>c</sup>, R.C. da Silva<sup>c</sup>

<sup>a</sup>Dep. de Conservação e Restauro and Centro do Vidro e da Cerâmica para as Artes, FCT-UNL, Quinta da Torre, 2829-516 Caparica, Portugal

<sup>b</sup>Monastery of Batalha, P-2440, Portugal

<sup>c</sup>Dep. Física, LFI, ITN, E.N.10, 2686-953 Sacavém, Portugal

## ARTICLE DATA

### Article history:

Received 16 July 2010

Received in revised form

1 December 2010

Accepted 7 December 2010

### Keywords:

Stained glass

Glass corrosion

Ion beam analysis

Raman

FTIR

## ABSTRACT

This paper reports the study of corrosion in two stained glass panels from the south aisle of Sta. Maria da Vitória monastery, at Batalha (Portugal), one depicting the Last Supper (dated from 1508), and the other one showing a saint (c. 1450). These panels exhibit extensive corrosion with darkening phenomena that are an impediment to their correct visualization, a source of major concern both to conservators and curators. By using external micro-beam Particle Induced X-ray Emission (PIXE) and Particle Induced Gamma Emission (PIGE) spectrometry, the elemental compositions of large fragments were obtained, enabling the selection of representative corroded areas, from which elemental distribution maps were produced by scanning. Calcium and potassium rich structures were found – at the surface and inside cavities in the glass – that were identified as oxalates and carbonates, by Raman microscopy and micro-FTIR. The dark spots present in the glass surfaces were found to be Zn and Pb rich. These findings indicate that the corrosion observed was due not only to reactions with atmospheric water and CO<sub>2</sub> but also with the oxalic acid secreted by micro-organisms. Furthermore, it did not result from reactions with atmospheric SO<sub>2</sub> or acid rain. The information obtained is relevant for a better understanding of the corrosion processes and products formed on the surface of these panels and therefore for the proper planning of much needed adequate conservation–restoration actions and appropriate display conditions.

© 2010 Elsevier Inc. All rights reserved.

## 1. Introduction

Due to the poor condition of the 15th century and early 16th century stained glass panels from the church aisles of the Monastery of Santa Maria da Vitória, at Batalha, Portugal, their permanent transfer to museum display after treatment was recommended. All panels from the north aisle were taken down, studied and treated between 1997 and 2008. It is now time to turn to the panels from the south aisle.

All the stained glass panels from the Monastery are largely affected by corrosion. This is an impediment to their correct visualization due to extensive loss of glass transparency and

darkening usually arising from the formation of micro-cracking of the hydrated surface layers [1,2]. The aim of this work was to analyse different corrosion morphologies that are present in these glass surfaces, since its identification is crucial to an adequate planning of conservation–restoration actions.

Two different panels were chosen: i) a figure with a nimbus dating between 1440 and 1480 AD (S07c) and ii) one panel, representing Saint John Evangelist, dated 1508 AD (S10a) (cf. Fig. 1).

Both panels were reassembled in the 19th century and, for that, fragments from several different panels were used [3]. The panels under study show a dramatic change in style, from the

\* Corresponding author. Tel./fax: +351 21 2948 322.

E-mail address: [mgv@fct.unl.pt](mailto:mgv@fct.unl.pt) (M. Vilarigues).

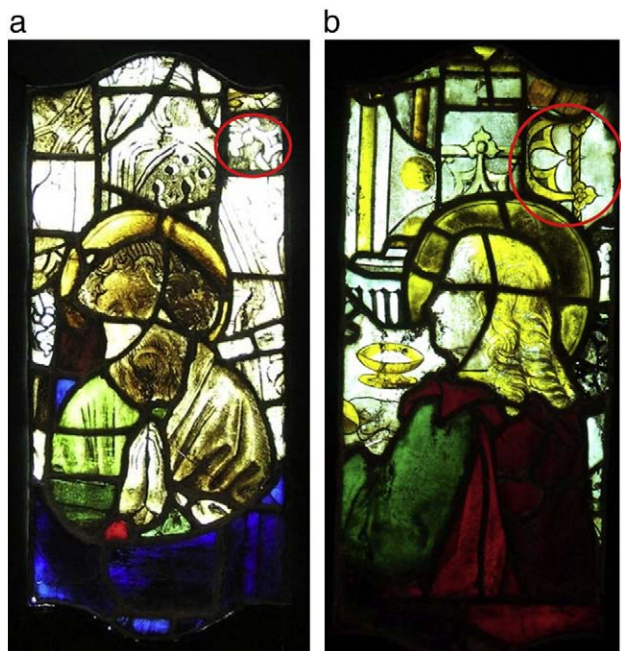


**Fig. 1 – Images of the panels under study (a) figure with a nimbus dating between around 1440 and 1480 (S07c) and (b) Saint John Evangelist dated 1508 (S10a) with the analysed fragments specified.**

schematic outline of compositions and figures, introduced in the Monastery workshop by Luís the German [4], to the soft realism of Master João [3]. Sheet glass manufacture is also different: most pieces in the earlier panel were cut from crown glass (made by spinning molten glass attached to an iron pontil

so that it spreads centrifugally into a sheet) whereas St. John's was carried out using mostly cylinder glass (made by blowing a hollow glass sphere, then swinging it vertically thus shaping it into a cylinder, which ends are cut off, then the resulting cylinder is cut lengthways, and laid flat).

Both panels are affected by corrosion that locally changes the glass composition and leads to the formation of compounds such as gypsum ( $\text{CaSO}_4 \cdot 2\text{H}_2\text{O}$ ) or calcium carbonate ( $\text{CaCO}_3$ ). Darkening phenomena, which cannot be found in subsequent stained glass produced for the Monastery between 1514 and the early 1530s, are also present. The main goals of this work was the characterisation and investigation of the compositional changes that result from corrosion and the darkening observed on the surface of these stained glasses. In the literature, this darkening has been assigned either to a change in the oxidation state of leached manganese and iron ions [5,6] or as a consequence of micro-organism activity [7]. As an attempt to overcome this problem, solutions of hydrazine hydrate [8–11] or mixtures of potassium iodide and hydrochloric acid [12] have been used to revert or prevent changes in the oxidation states of Mn and Fe ions. Both treatments are very aggressive to glass surfaces on account of both high and low pHs of the reagents used. Moreover, their application is limited to unpainted surfaces. In practice, a painted glass can be treated if the grisaille is conveniently protected with a film of a reversible polymer like Paraloid B72. However, this can only be effectively applied to contour and not to shaded areas. Another disadvantage of the above-mentioned procedures is the need to dismantle the panels. Pilot treatments using hydrazine hydrate followed by formic acid were monitored after up to around 15 years of their application and revealed scarce material change, especially in the case of the glass protected by primary corrosion gel layers [11].

**Table 1 – Composition of the glass of fragment 9 of panel S10a and fragment 7 of panel S07c determined both on the obverse and reverse of the panels, as well as inside the holes found in the glass surface of panel S10a and black points of S07c. These compositions were obtained by micro-PIXE and micro-PIGE analyses. Except for Cl the compositions are expressed as mass fractions ( $\times 100$ ) of the corresponding most common oxides.**

	Fragment 9 of panel S10a (1508)			Fragment 7 of panel S07c (1440–1480)		
	Obverse	Reverse	Hole	Obverse	Reverse	Black points
$\text{Na}_2\text{O}$	1.56	4.72	1.72	4.83	3.74	5.00
$\text{MgO}$	0.49	1.03	0.66	n.d	n.d	n.d
$\text{Al}_2\text{O}_3$	3.94	2.73	6.20	4.52	3.33	5.16
$\text{SiO}_2$	58.54	60.36	57.58	48.16	60.10	54.97
$\text{P}_2\text{O}_5$	2.06	2.36	2.03	2.38	3.87	1.94
$\text{SO}_3$	3.93	0.87	2.78	3.03	0.49	3.34
Cl	0.56	0.59	0.53	0.97	0.66	0.96
$\text{K}_2\text{O}$	4.40	4.58	0.23	13.19	14.85	4.37
CaO	17.84	19.77	1.75	17.31	10.12	10.11
$\text{TiO}_2$	0.14	0.11	0.31	0.21	0.13	0.20
MnO	0.94	1.05	6.38	1.18	1.12	1.07
$\text{Fe}_2\text{O}_3$	3.28	0.60	1.85	1.03	0.72	1.18
CoO	0.02	–	0.01	0.01	0.01	0.02
CuO	0.30	0.06	0.19	0.1	0.18	0.14
ZnO	0.17	0.53	1.00	0.73	0.65	2.73
$\text{As}_2\text{O}_3$	0.13	0.04	0.73	0.11	n.d	n.d
SrO	0.06	0.07	0.05	0.06	n.d	n.d
BaO	0.27	0.29	0.84	0.41	0.10	0.32
PbO	1.39	0.19	15.15	1.85	0.43	7.79

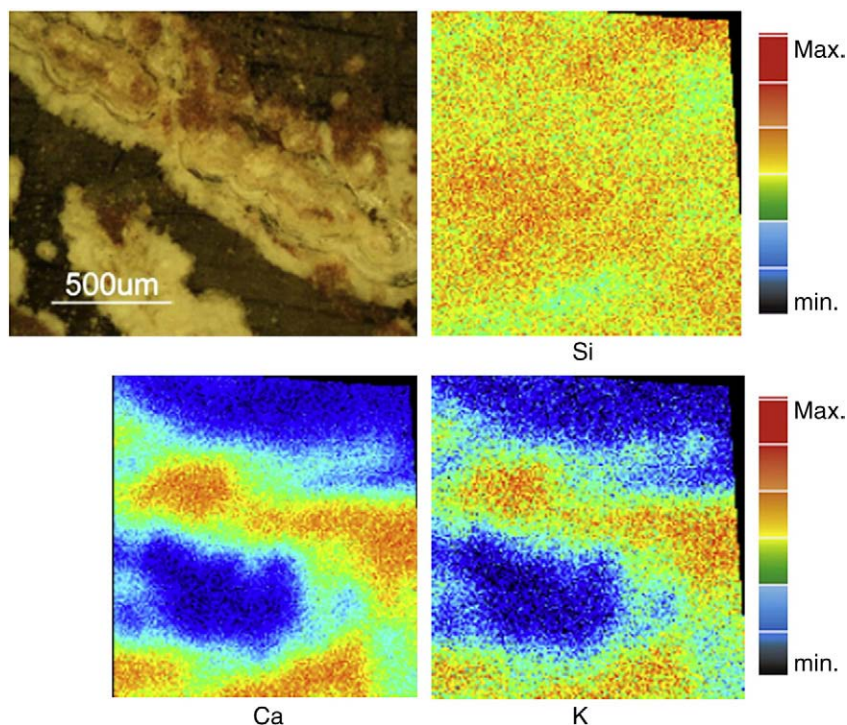


**Fig. 2 – Optical micrograph and representative 1 mm × 1 mm X-ray elemental distribution maps obtained from a corroded region of fragment 9 of panel S07c.**

The objects under study, were analysed through different techniques, namely Ion Beam Analytical techniques,  $\mu$ -FTIR and  $\mu$ -Raman spectroscopies.

Ion beam analysis, both in broad beam and focused beam, is a remarkable tool for the investigation of objects of cultural heritage [13], especially if that can be done at atmospheric pressure. In particular, the nuclear microprobe combines the analytical capabilities of essentially non-destructive spectroscopies, with mapping capabilities with micrometer lateral resolution. This combined information may contribute to a deeper understanding of the glass technology and its corrosion behaviour. The microprobe analyses in the external beam are performed without the need of sampling or coating, thus allowing the identifying of

the composition of the glass, paintings with grisailles and yellow silver stain, as well as the corrosion products without altering important historical material.

FTIR and RAMAN are two well-established techniques that have been successfully applied to the non-destructive characterization of art pieces and cultural heritage objects or artefacts [14,15].

## 2. Experimental

The external beam facility used in this work is an extension of the existing nuclear microprobe beam line that does not compromise its normal (in vacuum) operation. Nuclear analytical techniques were simultaneously used with the external beam, namely Particle Induced X-ray Emission (PIXE) in combination with Particle Induced Gamma Emission (PIGE), allowing quantitative determination of the elemental compositions of the glass, painted layers and corrosion products. The excitation of the target atomic and nuclear levels yielding characteristic X- and gamma-rays was provided by a 2 MeV proton beam from a 2.5 MV Van de Graaff accelerator, focused by an Oxford Microbeams OM50 triplet quadrupole system onto the target placed 3 mm away from the 100 nm thick  $\text{Si}_3\text{N}_4$  extraction window. The on target focused 1 nA beam spot was measured to be  $70 \times 75 \mu\text{m}^2$  in air, at normal atmospheric pressure. The OM-DAQ computer controlled beam steering allowed scanning target areas up to  $1000 \times 1000 \mu\text{m}^2$ , in synchronism with the acquisition of the spectral data.

The collection of PIXE and PIGE spectra was performed using a  $30 \text{ mm}^2$  Roentec X-Flash® SDD X-ray detector with 135 eV energy resolution and a large volume ORTEC HPGc detector with

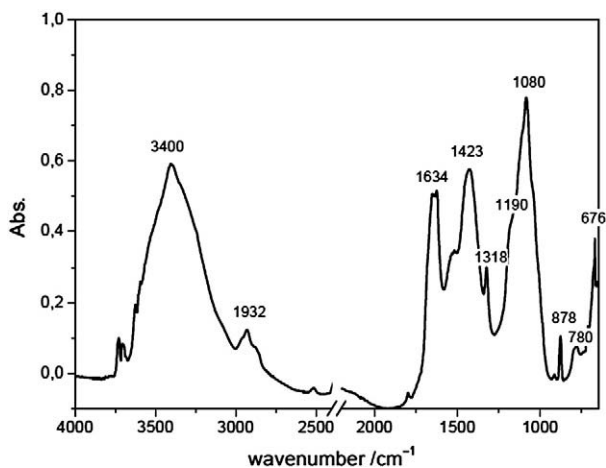


**Fig. 3 – FTIR spectra of several samples, exhibiting different corrosion products: carbonates and oxalates.**

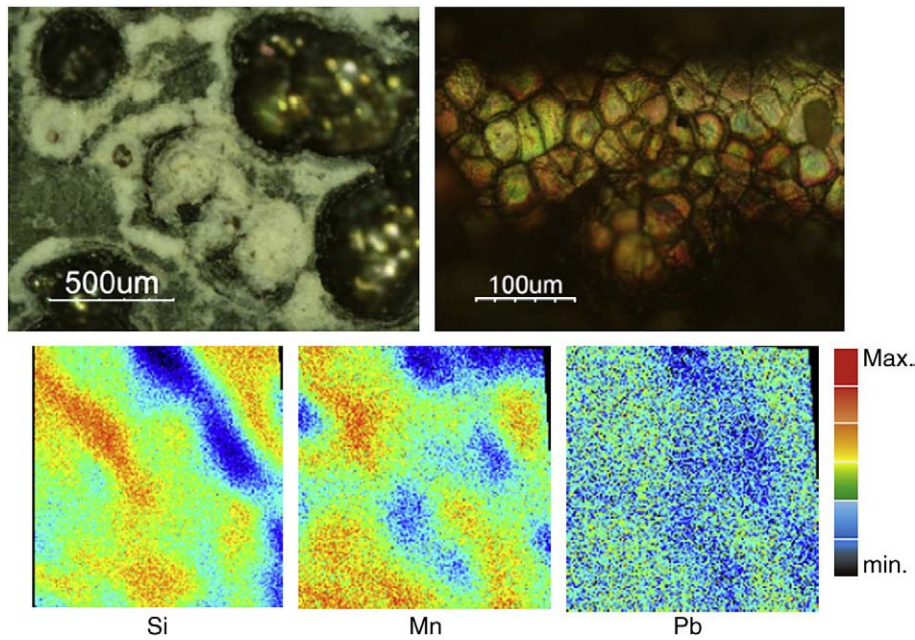


**Fig. 4 – Optical micrograph and representative 1 mm × 1 mm X-ray elemental distribution maps obtained from a corroded region with holes from fragment 9 of panel S10a.**

45% efficiency and 1.9 keV energy resolution, both placed at 45° angles to the incoming beam direction.

The PIXE spectra were analysed using the AXIL [16] program for line deconvolution and DATPIXE [17] for quantification. The detection and quantification of elements of  $Z \leq 12$  was made through PIGE, by measuring the yields of the 440 keV and 585 keV gamma lines from proton capture reactions with Na and Mg respectively. The results were constantly compared for each sample with those obtained using Corning glass reference standards.

The corrosion products were identified by  $\mu$ -FTIR technique using a Nicolet Nexus spectrometer equipped with a Continuum microscope, in either one of two modes: in reflectance using an Attenuated Total Reflectance (ATR) slide-on accessory with Si crystal; or in transmittance using a diamond compression cell. Micro-Raman analysis was also performed to study the differences between grisaille and browning, which exhibit different morphologies as seen by optical microscopy. This was carried out using a Labram 300 Jobin Yvon spectrometer, equipped with a 17 mW He–Ne laser operating at 632.8 nm. The laser beam was focused either with a 50× or a 100× Olympus

objective lens, its power controlled with the aid of a set of neutral density filters of optical densities in the range of 0.3 to 2.

### 3. Results and Discussion

Table 1 summarises the compositions of analysed representative stained glass fragments. It is to be noticed the differences that were found in the composition of the glass in reverse and obverse sides, and that these compositions were determined at the surface. In spite of this, fragments from panel S07c may be classified as potash glasses with high alkali content, while fragments from the 16th century panel (S10a) have a lower content in potash. These results agree with the compositions found in the previous studies for other panels of the same provenance and period [1,2,18]. The production of stained glass in Monastery of Batalha followed the central European tradition, with the implication that ashes from continental plants (richer in potassium) were used [19]. It is to be noticed that according to the literature that potash-rich glasses are more susceptible to aqueous corrosion than are soda-rich glasses [20].

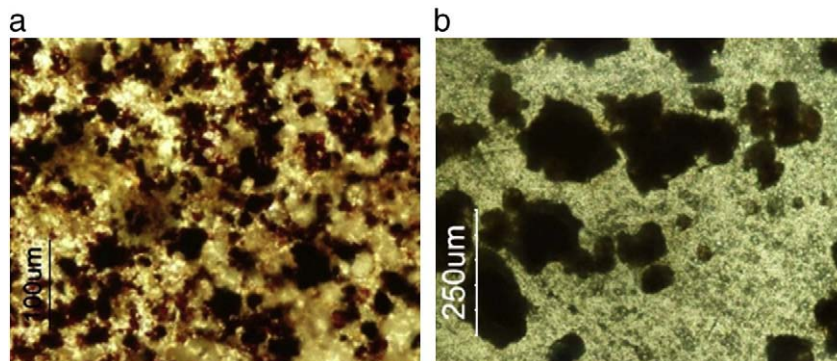


**Fig. 5 – Optical micrograph of (a) region painted with grisaille and (b) opacified region of fragment 7 of panel S07c.**

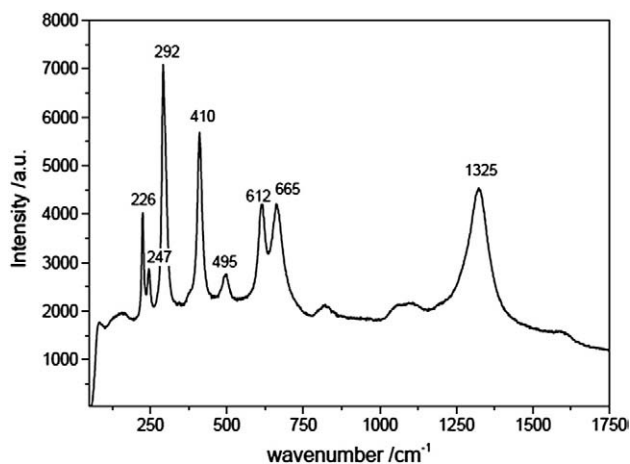


Fig. 6 – Raman spectra of grisaille from fragment 7 of panel S07c.

White corrosion products, as the ones shown in the optical micrograph in Fig. 2, are spread all over the glass surfaces. The corresponding elemental maps obtained by external micro-PIXE analysis (cf. Fig. 2) show enrichment in Ca and K contents. This enrichment is in accordance with the results of micro-FTIR analysis (Fig. 3) that reveals the presence of Ca and K compounds: carbonates and oxalates. In fact, the bands located at wave numbers  $1190\text{ cm}^{-1}$  and  $1080\text{ cm}^{-1}$  in the FTIR spectrum

are assigned to vibrations of Si–O–Si and Si–O<sup>-</sup> groups, respectively [21,22]. The existence of these two bands is characteristic of glasses with high content of alkaline and alkaline earth ions. The bands located between wave numbers  $600\text{ cm}^{-1}$  and  $1700\text{ cm}^{-1}$  are consistent with the presence of carbonates and oxalates in the analysed surfaces. According to the literature, the band located at  $1423\text{ cm}^{-1}$  and the peaks at  $878\text{ cm}^{-1}$  and  $676\text{ cm}^{-1}$ , are assigned to the asymmetric stretching, to the out-of-plane bending and to the in-plane bending in  $\text{CO}_3^{2-}$  groups, respectively [21], while those at  $1634\text{ cm}^{-1}$  (main anti-symmetric carbonyl stretching),  $1318\text{ cm}^{-1}$  (secondary carbonyl stretching mode) and  $780\text{ cm}^{-1}$  indicate the presence of oxalates [22]. Also to be noticed is the broad band around  $3400\text{ cm}^{-1}$  attributed to the vibrations of the OH<sup>-</sup> group, thus indicating a high level of hydration of the glass surface [21]. These findings are consistent with glass corrosion mechanisms [20,22]: corrosion starts when the surface of glass is exposed to water (e.g. moisture or rain water), alkali and alkaline earth ions leaching out and being replaced by hydronium ions, thus forming a hydrated layer at the glass surface. This layer can retract and yield, creating fissures through which the solution can reach the inner glass, allowing the alteration to propagate further. The leached cations can react with atmospheric gases, particularly  $\text{CO}_2$  crystallizing at the surface in the form of carbonates. Other compounds, e.g. gypsum ( $\text{CaSO}_4 \cdot 2\text{H}_2\text{O}$ ) or syngenite ( $\text{K}_2\text{Ca}(\text{SO}_4)_2 \cdot \text{H}_2\text{O}$ ), were not found indicating that

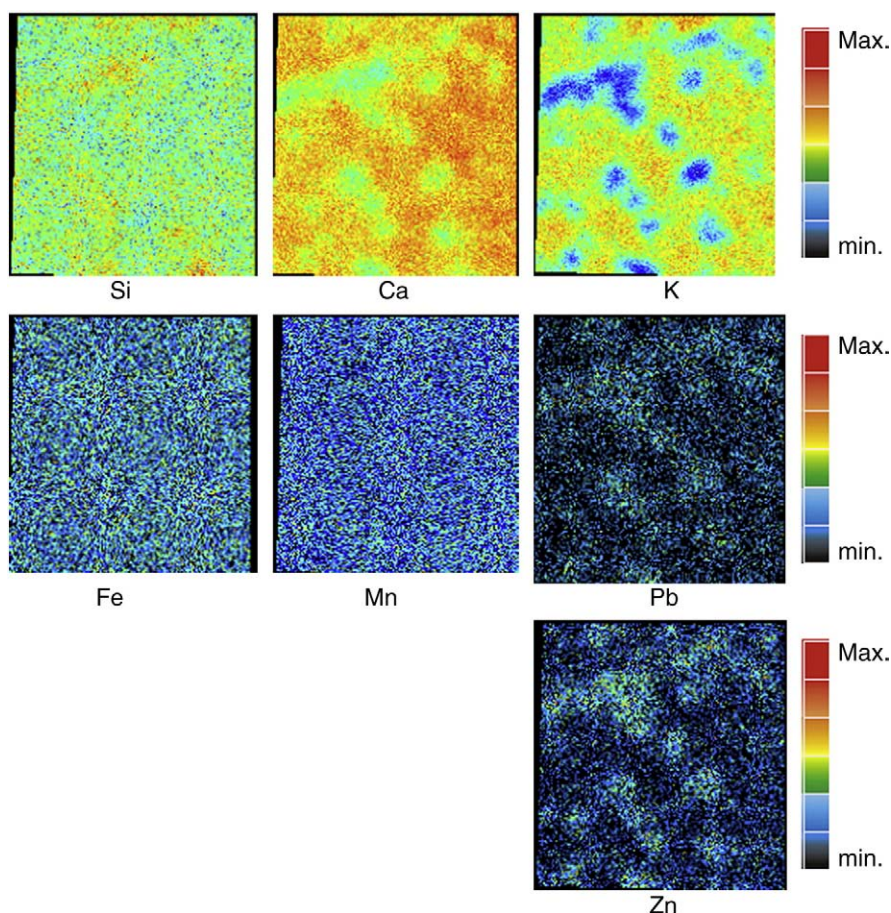


Fig. 7 –  $1\text{ mm} \times 1\text{ mm}$  X-ray elemental distribution maps obtained from an opacified region of fragment 7 of panel S07c.

atmospheric SO<sub>2</sub> did not contribute to corrosion. As to the oxalates it is known that these are formed by the action of oxalic acid secreting microorganisms in the glass surface that metabolically convert carbonates into oxalates [23]. This conversion may further accelerate the corrosion by locally changing the pH.

Other pathologies were found in several fragments from these two panels. The examination of the surfaces of fragments from panel S10a under the microscope revealed the presence of several holes that may interconnect, creating channels where loss of material is visible. Micro-PIXE analyses of these cavities show enrichment in lead and manganese, decreased concentrations of calcium and potassium, but no significant variation in the Si contents (cf. Fig. 4 and Table 1).

The existence of these cavities is a consequence of glass corrosion. In places of preferential attack, leaching and redistribution of soluble components (mainly alkali and alkaline earth) lead to the partial dissolution of the silicate network and formation of micro-craters (pits) in the surface. When a fairly large volume is affected, the different rheologies of unaltered glass and corroded layers give rise to a network of radial micro fractures [24]. The K, Ca, Pb and transition-metal ions move to the surface, with only K and Ca passing to the solution, Ca being redeposited later on the surface of the glass in the form of carbonates [25].

In contrast, some fragments of panel S07c exhibited darker regions (as shown in the optical micrograph in Fig. 5), which are difficult to distinguish from the grisaille. Darkening like this has been originally explained by some authors as associated with the oxidation of manganese [5–7]. Raman and micro-PIXE results obtained from grisaille and darkened regions are depicted in Figs. 6 and 7 respectively. The Raman spectrum of Fig. 6 matches that of  $\alpha$ -Fe<sub>2</sub>O<sub>3</sub> (hematite) quite well — the set of peaks located at 226 cm<sup>-1</sup> and 495 cm<sup>-1</sup> assigned to A<sub>1g</sub>, and those at 247 cm<sup>-1</sup>, 292 cm<sup>-1</sup>, 410 cm<sup>-1</sup>, 612 cm<sup>-1</sup> and 1325 cm<sup>-1</sup> to E<sub>g</sub> transitions respectively. Even the disorder-induced activation of the IR-active mode at 665 cm<sup>-1</sup> is present [26]. No Raman signal was obtained from the darkened regions confirming that the nature of these is distinct from the grisaille.

An analyses of the micro-PIXE results presented in Fig. 7 reveal that these darkened regions are Zn and Pb richer, highly depleted in K, but with similar contents of Mn and Fe. Thus, in spite that a mere change in the oxidation state of manganese, as described in the literature [5–7] cannot be excluded, the observed darkening is certainly associated with the formation of these Zn–Pb rich structures. Furthermore, their morphological appearance, the fact that they reside “inside” the glass matrix and that both Zn and Pb show a roughly similar 4-fold increase in concentration, suggests an internal source and common transport–precipitation mechanism. Although the sets of Pb–Zn and K–Ca PIXE maps of Fig. 7 are not inconsistent with a phase separation by spinodal decomposition, it is difficult to understand that the Mn and Fe distributions remain unaffected by such process. Thus, the origin of such enrichment may be the simple ion exchange and transport associated with the leaching mechanisms of corrosion, leading to precipitation and growth into these structures. Unfortunately, the chemical state of Zn and Pb in these dark spots could not be established, so the exact mechanism at action remains unknown. The existence of Zn at the surface of the corroded stained glasses is

rare and, to the best of our knowledge, has only been reported in glasses from Asnières sur Vesgres in the form of K<sub>2</sub>Zn(SO<sub>4</sub>)<sub>2</sub> [27].

#### 4. Conclusions

The combined use of nuclear microprobe techniques with  $\mu$ -FTIR and  $\mu$ -Raman analyses, allowed the characterization of corrosion effects and/or products observed at the surface of the medieval stained glasses studied.

Using an external nuclear microprobe, evidence was found for the development of Ca and K rich structures both at the surface and inside the holes that were formed in the glass. These holes were characterized for the first time with a non-destructive technique and directly on the glass piece, i.e. without sampling, and were identified to be composed of carbonates and oxalates through  $\mu$ -FTIR analysis. The finding of these compounds – and the absence of others (e.g. gypsum or syngenite) characteristic of attack by atmospheric SO<sub>2</sub> – point to a corrosion due to high humidity levels and further reactions with atmospheric CO<sub>2</sub> and oxalates of micro-biological origin.

Another surface pathology that was studied in this work was the existence of dark spots in the glass surfaces. Visually these spots may be wrongly identified as grisaille, but the micro-PIXE analysis in association with micro-Raman spectroscopy allowed characterizing these spots as rich in Zn and Pb, but clearly distinct from grisaille. Although possibly a consequence of ion exchange associated with localized leaching, precipitation and growth the precise mechanism(s) responsible for these formations remain as yet an open question.

#### Acknowledgment

This project is supported by Fundação para a Ciência e Tecnologia (FCT).

We thank to IGESPAR for allowing us to analyse the samples from Monastery of Batalha.

#### REFERENCES

- [1] Vilarigues M, Fernandes P, Alves LC, da Silva RC. Stained glasses under the microprobe: a window into history. *Nucl Instrum Methods B* 2009;267:2260–4, doi:10.1016/j.nimb.2009.03.049.
- [2] Fernandes P, Vilarigues M, Alves LC, da Silva RC. Stained glass from Monastery of Batalha: non-destructive characterization of glass and paintings. *J Cult Herit* 2008;9(Supplement 1):e5–9.
- [3] Redol P. O Mosteiro da Batalha e o Vitral em Portugal nos Séculos XV e XVI. Batalha: Câmara Municipal da Batalha; 2003.
- [4] Hess D. In search of Luís Alemão. Stained glass in Germany from 1400 till 1460 and the fragments in Batalha. *O Vitral: história, conservação e restauro, Proceedings of International Stained Glass Meeting, Batalha, 27–29th April, 1995* 972-8087-69-1; 2000. p. 44–53. IPPAR.
- [5] Marschner H. Verwitterung und Konservierung von historischem Fensterglas. *Glaskonservierung. Historische Glasfenster und ihre Erhaltung*, 32. Arbeitsheft des Bayerischen Landesamtes für Denkmalpflege; 1985. p. 123–64.
- [6] Müller W, Pouillon H, Bochynek G, Mehne H. Extreme Dunkelung von Glasmalereien. *Glastech Ber* 1986;59:96–102.

- [7] Oriol G, Warscheid T, Bousta F, Loisel C. Incidence bactérienne dans les phénomènes de brunissement des vitraux anciens. *Actual Chim* 2007;312/313:34–9.
- [8] Drachenberg E. Versuche zur Wiederherstellung der völlig lichtundurchlässig gewordenen Glasmalereien aus Marienstern. *CV Newsl* 1984;37/38:4.
- [9] Müller W. Versuche zur Wiederaufhellung stark gedunkelter mittelalterlicher Gläser. *Glaskonservierung. Historische Glasfenster und ihre Erhaltung*, 32. Arbeitsheft des Bayerischen Landesamtes für Denkmalpflege; 1985. p. 80–1.
- [10] Fitz S. Ergebnisse des Forschungsvorhabens ‘Zur Einwirkung von Luftunreinigungen auf Glasgemälde. *Glaskonservierung. Historische Glasfenster und ihre Erhaltung*, 32. Arbeitsheft des Bayerischen Landesamtes für Denkmalpflege; 1985. p. 88–92.
- [11] Müller W. *Verbräunte mittelalterliche Glasmalereien. Verfahren zur Aufhellung*. Leipzig: Edition Leipzig; 2002.
- [12] Pinto A. Le problème du manganèse oxydé dans les verres anciens: recherche et expérimentation. *Vitrea* 1991;7:27–33.
- [13] Calligaro T. PIXE in the study of archaeological and historical glass. *X-Ray Spectrom* 2008;37:169.
- [14] Ciliberto E, Spoto G, editors. *Modern analytical methods in art and archaeometry*. John Wiley & Sons; 2000.
- [15] Stuart Barbara H. *Analytical techniques in materials conservation*. John Wiley & Sons; 2007.
- [16] Grime GW. *Nucl Instr Meth B* 1996;109–110:170.
- [17] Reis MA, Alves LC. DATPIXE, a computer package for TPIXE data analysis. *Nucl Instrum Meth Phys Res B* 1992;68(1-4):300–4, doi:10.1016/0168-583X(92)96098-J.
- [18] Vilarigues M, da Silva RC. Ion beam and Infrared analysis of medieval stained glass. *Appl Phys A* 2004;79:373–8.
- [19] Caen JM. *The production of stained glass in the county of Flanders and the Duchy of Brabant from the 15th to the 18th centuries: materials and techniques*. Antwerpen: Brepols Publishers 978-1-905375-64-6; 2009.
- [20] Clark DE, Zaitos BK, editors. *Corrosion of glass, ceramics and ceramic superconductors*. Noyes Publications 978-0-8155-1283-7; 1992.
- [21] Abo-Naf SM, El Batal FH, Azooz MA. Characterization of some glasses in the system  $\text{SiO}_2$ ,  $(\text{Na}_2\text{O RO})$  by infrared spectroscopy. *Mater Chem Phys* 2002;77(3):846–52.
- [22] Vilarigues M, da Silva RC. Characterization of potash–glass corrosion in aqueous solution by Ion Beam and IR Spectroscopy. *J Non-Cryst Solids* 2006;352:5368–75.
- [23] Anjian Xie, Yuhua Shen, Dong Ma, Fangzhi Huang, Lingguang Qiu, Shikuo Li, et al. Growth of calcium oxalate crystals induced by complex films containing biomolecules. *Cryst Res Technol* 2007;42(7):667–72.
- [24] Sterpenich J, Libourel G. Using stained glass windows to understand the durability of toxic waste matrices. *Chem Geol* 2001;174(1–3):181–93.
- [25] Vilarigues M, da Silva RC. The effect of Mn, Fe and Cu ions on potash–glass corrosion. *J Non-Cryst Solids* 2009;355:1630–7.
- [26] Bersani D, Lottici PP, Montenero A. Micro-Raman investigation of iron oxide films and powders produced by sol–gel syntheses. *J Raman Spectrosc* 1999;30:355–60.
- [27] Jorba M. *La pollution atmosphérique et la corrosion des verres. Stained glass: conservation of monumental stained and painted glass*. ICOMOS 955-613-044-6; 1993. p. 218–27.